

Article

Research on a Wide-Output Resonant Converter with Multi-Mode Switching

Yu Gu ^{1,2,*}, Xiaofeng Zhang ³, Bingyang Wang ¹, Zhangwen Jia ³ and Anshou Li ²

¹ Power Electronics and Motion Control Research Center, Harbin Institute of Technology (Shenzhen), Shenzhen 518055, China

² Department of Mathematics and Theories, Peng Cheng Laboratory Shenzhen, Shenzhen 518055, China

³ China Academy of Space Technology, Beijing 100094, China

* Correspondence: guyu@hit.edu.cn

Abstract: In this article, a resonant converter based on a series-parallel self-adjusting rectifier structure is proposed. By changing the driving signal of the switch, the converter has four working modes: full-bridge structure frequency modulation control, full-bridge structure phase-shift control, half-bridge structure frequency modulation control and half-bridge structure phase-shift control. The newly proposed resonant converter retains the soft switching characteristics of the LLC resonant converter and the mode switching can be completed only through software control without adding additional switches. Different modes correspond to different gain ranges. By changing the control strategy of the modes, the newly proposed converter can meet the design requirements of wide output. Finally, an experimental prototype with an input voltage of 25 V and an output voltage of 9 V to 35 V is built. The experimental results prove the correctness of the wide output characteristics of the converter proposed in the article and, in the four operating modes, it can realize zero-voltage turn-on of the active switch on the primary side and zero-current turn-off of the rectifier diode on the secondary side, which preserves the high efficiency of the resonant converter.



Citation: Gu, Y.; Zhang, X.; Wang, B.; Jia, Z.; Li, A. Research on a Wide-Output Resonant Converter with Multi-Mode Switching. *Energies* **2022**, *15*, 6754. <https://doi.org/10.3390/en15186754>

Academic Editors: Yam P. Siwakoti and Jagabar Sathik Mohammed

Received: 31 July 2022

Accepted: 13 September 2022

Published: 15 September 2022

Publisher's Note: MDPI stays neutral with regard to jurisdictional claims in published maps and institutional affiliations.

Keywords: series-parallel; self-adjusting; soft switching; wide output; multi-mode; resonant converter

1. Introduction

Since the LLC resonant converter was proposed, it has been quickly applied to all walks of life because of its high efficiency and high power-density [1]. Figure 1 shows the circuit topology of the LLC resonant converter. The LLC resonant converter utilizes the characteristics of the resonant element to control the magnitude of the output voltage by changing the frequency of the square wave voltage input to the tank circuit. The parameters of the resonant element determine the gain curve of the converter under frequency modulation (FM) control. When the value of the magnetic inductance L_m is smaller, the gain range of the resonant converter is wider and the turn-off loss and conduction loss introduced into the circuit will be larger [2,3]; the two requirements of high efficiency and wide gain are difficult to coexist at the same time.

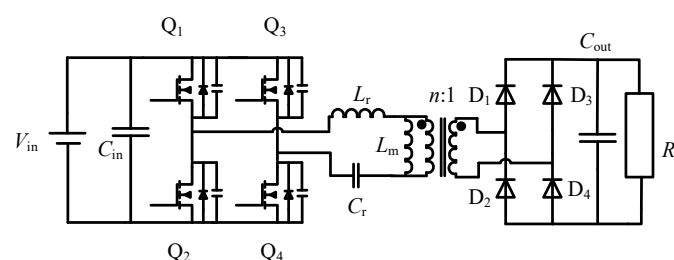


Figure 1. LLC resonant converter circuit diagram.



Copyright: © 2022 by the authors. Licensee MDPI, Basel, Switzerland. This article is an open access article distributed under the terms and conditions of the Creative Commons Attribution (CC BY) license (<https://creativecommons.org/licenses/by/4.0/>).

Using FM control alone, the output voltage of the converter decreases as the switching frequency increases. However, a too-high switching frequency will not only increase the loss of the circuit but also make the selection of the device more stringent. Some scholars have proposed a hybrid control strategy of frequency modulation combined with phase shifting [4,5]. When the switching frequency increases to the resonant frequency, the switching frequency is fixed and the output voltage is changed by controlling the phase shifting angle of the switch. The minimum phase shift angle can be reduced to 0, thus expanding the output voltage range of the resonant converter.

A too-small phase shift angle will also increase losses in the circuit. Reference [6] proposed a variable mode control strategy to achieve the purpose of wide output. In this control mode, when the input voltage gradually increases, the circuit will work in three operating modes in turn: full-bridge frequency modulation, full-bridge phase shift and half-bridge frequency modulation. This control strategy has been able to provide a considerable gain range, but when the required gain range is further expanded, it will be required to continue to increase the switching frequency, or to redesign the turns ratio of the transformer [7,8].

To further widen the output voltage range of the resonant converter, a novel wide-output resonant converter is proposed here. Figure 2 shows the main circuit part of the converter, and Q_1 – Q_6 are active switches that constitute three inverter arms. The diodes D_1 – D_6 are the body diodes of Q_1 – Q_6 , and C_1 – C_6 are the parasitic capacitances of each active switch, respectively. There are two transformers, T_1 and T_2 , with the same transformation ratio in the circuit. On the primary side of the transformer, there are resonant capacitors C_{r1} , C_{r2} , resonant inductors L_{r1} , L_{r2} and excitation inductors L_{m1} , L_{m2} . The corresponding resonant parameters in the two tank circuits are the same. On the secondary side of the transformer, D_{R1} – D_{R6} form a new series-parallel self-adjusting rectifier structure.

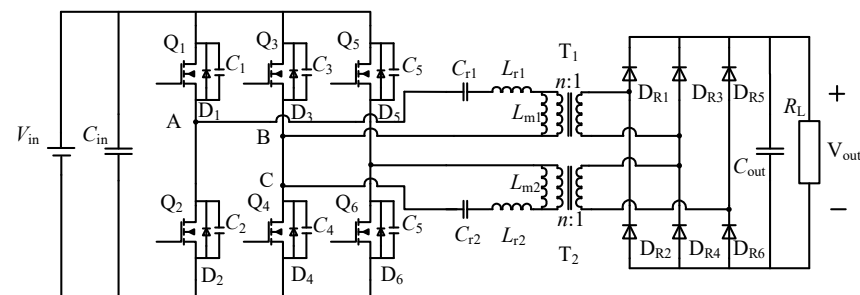


Figure 2. New wide output resonant converter circuit diagram.

2. Analysis of Each Working Mode of the Converter

In the new resonant converter proposed in this paper, according to the structural difference between the full-bridge and the half-bridge of the inverter unit and the difference in frequency modulation and phase shift in the control methods, the new resonant converter has four operating modes, followed by the full-bridge frequency modulation mode, full-bridge phase-shift mode, half-bridge FM mode and half-bridge phase-shift mode. Each operating mode has its own corresponding gain range.

2.1. Full-Bridge FM Mode

In the full-bridge FM mode, the driving waveforms of switches Q_1 , Q_4 and Q_5 are the same and the driving waveforms of switches Q_2 , Q_3 and Q_6 are also the same. The two sets of switches are complementarily turned on, providing square wave voltages with the same phase and an amplitude of $\pm V_{in}$ for the two tank circuits. The rectified currents output by the secondary sides of the two transformers are also of the same phase and the same amplitude, so D_{R3} and D_{R4} in the rectifier bridge do not work within one switching cycle. In the full-bridge FM mode, the main circuit can be equivalent to two LLC resonant converters, the input terminals are connected in parallel and the output terminals are connected in series, as shown in Figure 3. The gain range of the resonant converter in this

mode is twice that of a single full-bridge LLC resonant converter under FM control. The main waveform diagram in full-bridge FM mode is shown in Figure 4.

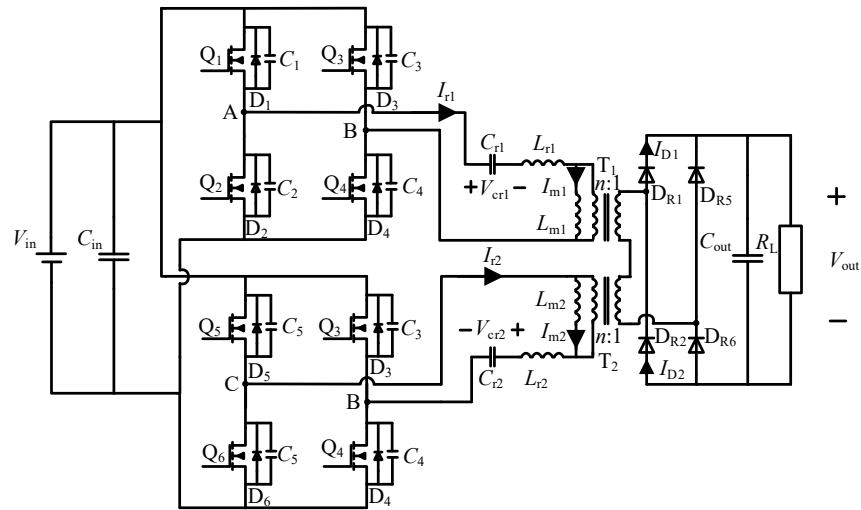


Figure 3. Equivalent circuit diagram of full-bridge FM mode and full-bridge phase-shift mode.

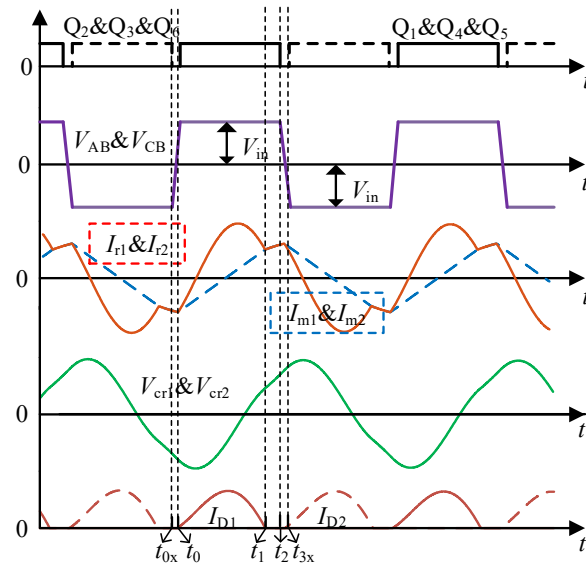


Figure 4. Main working waveform diagram of full-bridge FM mode.

2.2. Full-Bridge Phase Shift Mode

In the full-bridge phase-shift mode, the driving waveforms of the inverter bridge arm composed of switches Q_1 and Q_2 and the inverter bridge arms composed of switches Q_5 and Q_6 have the same timing sequence, and lag behind those composed of switches Q_3 and Q_4 . A phase shift angle is generated for phase shift control and changes the size of the output voltage. At this time, the input square wave voltages of the two tank circuits are also the same, and the equivalent circuit diagram of the main circuit is the same as the equivalent circuit diagram in the full-bridge frequency modulation mode. The gain of the circuit is twice that of a single full-bridge LLC resonant circuit under phase-shift control. The main waveforms in full-bridge phase-shift mode are shown in Figure 5.

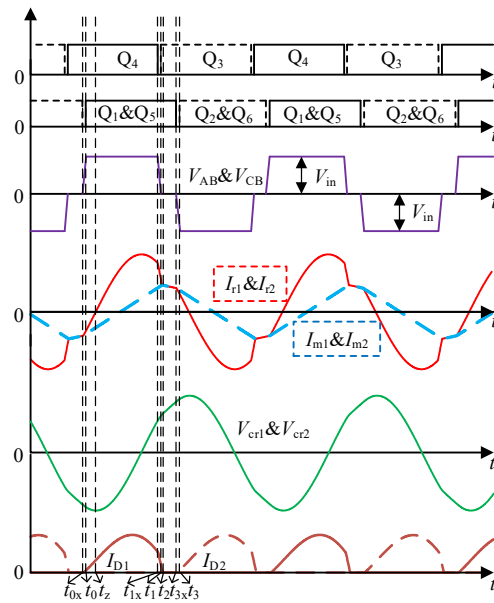


Figure 5. Main working waveform diagram of full-bridge phase-shift mode.

2.3. Half-Bridge FM Mode

In the half-bridge frequency modulation mode, the switch Q_4 is kept on, the switch Q_3 is kept off and the remaining four switches work in the frequency modulation control. The input square wave voltages of the two tank circuits are still the same in amplitude and phase, so the secondary side rectifier diodes D_{R3} and D_{R4} do not work all the time. The main circuit can be equivalent to two half-bridge LLC resonant circuits with inputs in parallel and outputs in series, as shown in Figure 6. In the half-bridge FM mode, the effective value of the input voltage of the tank circuit is half that of the full-bridge FM mode in one switching cycle, and its gain is naturally reduced to 1/2. The main waveforms in the half-bridge FM mode are similar to those in the full-bridge FM mode.

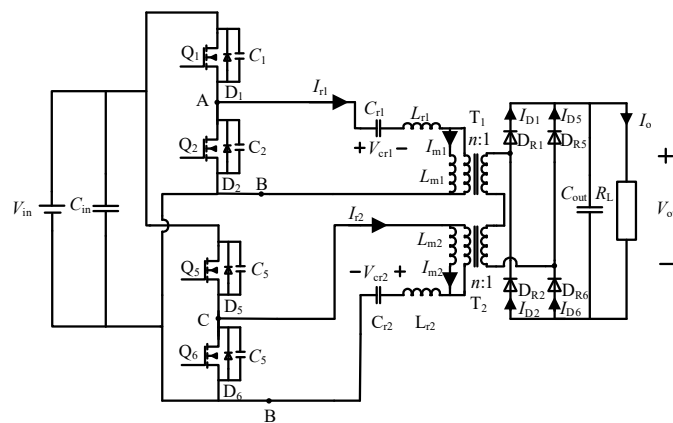


Figure 6. Equivalent circuit diagram of the half-bridge inverter mode.

2.4. Half-Bridge Phase Shift Mode

In the half-bridge phase-shift mode, the switch Q_4 is kept on and the switch Q_3 is kept off. A certain phase angle is generated between the inverter bridge arm composed of switches Q_1 and Q_2 and the drive waveform of the inverter bridge arm composed of switches Q_5 and Q_6 . At this time, the equivalent circuit diagram of the main circuit is shown in Figure 7. Although the input terminal can still be regarded as the input of two half-bridge LLC resonant converters in parallel, the phase of the input square wave voltage V_{AB} and V_{CB} of the two tank circuits is no longer consistent and the output of the transformer is not always in series. The size of the phase shift angle determines the time for the output of the

two transformer secondary sides to work in series and the time for a single transformer to independently transmit energy in half a switching cycle, and then controls the equivalent turns ratio of the transformer to change the output voltage. The main working waveform diagram in the half-bridge phase-shift mode is shown in Figure 8.

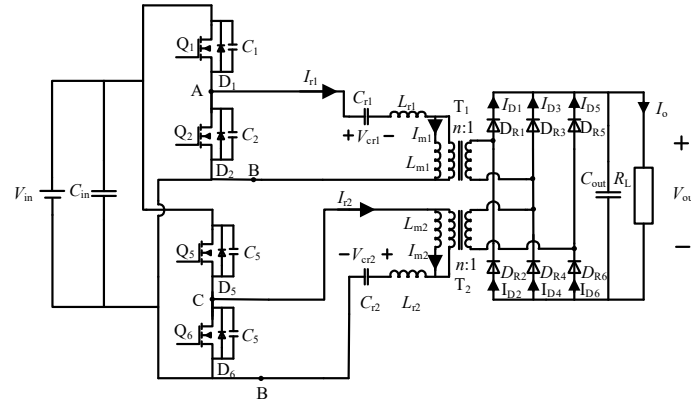


Figure 7. Equivalent circuit diagram for the half-bridge phase-shift mode.

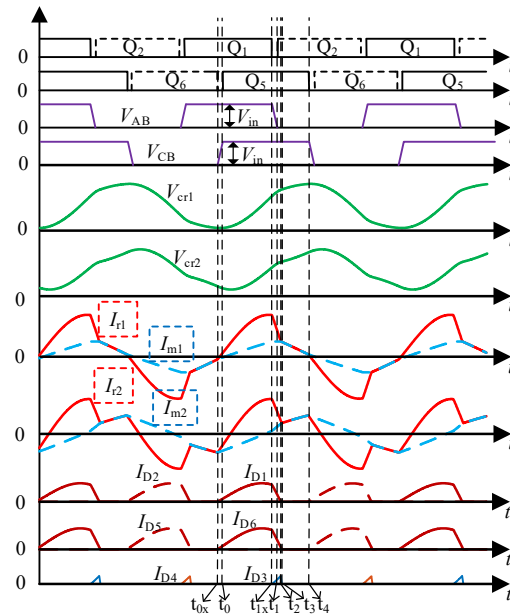


Figure 8. Main working waveform diagram of half-bridge phase-shift mode.

The specific working states of full-bridge LLC resonant converters under frequency modulation control or phase-shift control and half-bridge LLC resonant converters under frequency modulation control have been described in detail in much of the literature, so only the half-bridge phase-shift control mode is analyzed here.

1. Before time t_{0x} (Figure 9a), the switches Q_1 and Q_6 are turned on, and Q_2 and Q_5 are turned off. The voltage at the input terminal of resonance tank 1 is $V_{AB} = V_{in}$, and the voltage at the input terminal of resonance tank 2 is $V_{CB} = 0$. The resonant current is equal to the value of the excitation current, there is no energy transfer on the primary and secondary sides and the six diodes on the secondary side are all turned off.
2. In the $[t_{0x}, t_0]$ stage (Figure 9b) at t_{0x} , the switch Q_6 is turned off and the resonant current I_{r2} charges the capacitor C_6 and discharges the capacitor C_5 until the capacitor voltage across C_6 is charged to the input voltage V_{in} , and C_5 is also discharged completely; the switch tube Q_5 is ready for zero-voltage turn-on. At this time, the resonant current I_{r2} continues to flow through the body diode D_2 of Q_6 . The switch on bridge arm 3 has no action.

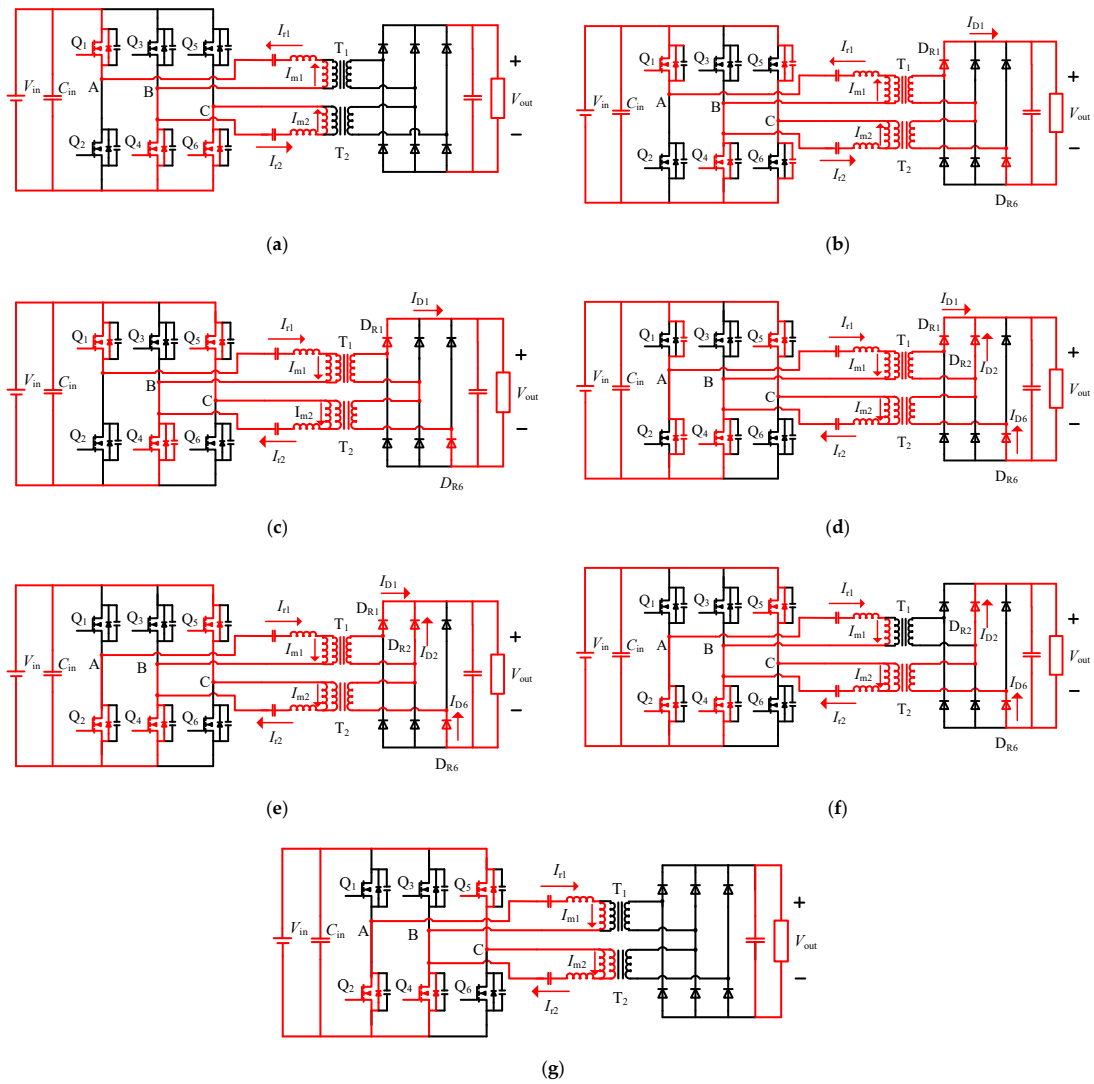


Figure 9. Main circuit diagram of each stage of the half-bridge phase-shift mode.

The input terminal voltage V_{CB} of tank circuit 2 increases from 0, and the resonant current I_{r2} starts to rise. Because the current difference between the resonant current and the excitation current is generated, the energy is transferred from the primary side of the transformer to the secondary side, the diodes D_1 and D_6 are turned on, the excitation inductances L_{m1} and L_{m2} are both clamped by $nV_{out}/2$ and the excitation current increases linearly. Resonant current I_{r2} of tank circuit 1 also begins to rise and the outputs of the two transformers are connected in series.

3. $[t_0, t_{1x}]$ stage (Figure 9c) at t_0 , the switch Q_5 is turned on at zero voltage, the voltage $V_{CB} = V_{in}$ is applied to the input of tank circuit 2, the inputs of the two tank circuits are connected in parallel, and the power supply charges the resonant capacitor. The resonant currents I_{r1} and I_{r2} gradually increase from negative values to 0 and keep rising, and the primary side continues to transfer energy to the secondary side. The expressions of v_{cr1} , v_{cr2} , i_{r1} , i_{r2} , i_{m1} , i_{m2} in this stage are as follows.

Tank circuits 1 and 2:

$$v_{cr1\&2}(t) = V_{in} - \frac{n \cdot V_{out}}{2} + i_{r1\&2}(t_0) \cdot \sqrt{\frac{L_r}{C_r}} \cdot \sin\left[\sqrt{\frac{1}{L_r \cdot C_r}}(t - t_0)\right] + [v_{cr1\&2}(t_0) - (V_{in} - \frac{n \cdot V_{out}}{2})] \cdot \cos\left[\sqrt{\frac{1}{L_r \cdot C_r}}(t - t_0)\right] \quad (1)$$

$$i_{r1\&2}(t) = i_{r1\&2}(t_0) \cdot \cos\left[\sqrt{\frac{1}{L_r \cdot C_r}}(t - t_0)\right] - [v_{cr1\&2}(t_0) - (V_{in} - \frac{n \cdot V_{out}}{2})] \cdot \sqrt{\frac{C_r}{L_r}} \cdot \sin\left[\sqrt{\frac{1}{L_r \cdot C_r}}(t - t_0)\right] \quad (2)$$

$$i_{m1\&2}(t) = i_{m1\&2}(t_0) + \frac{n \cdot V_{out}}{2 \cdot L_m} \cdot (t - t_0) \quad (3)$$

4. $[t_{1x}, t_1]$ stage (Figure 9d) at t_{1x} , the switch Q_1 is turned off and the resonant current I_{r1} charges the capacitor C_1 and discharges the capacitor C_2 until the capacitor voltage across C_1 is charged to the input voltage V_{in} , and C_2 is also discharged, the switch Q_2 is ready for zero-voltage turn-on, and the resonant current I_{r1} continues to flow through the body diode D_1 of Q_1 . The switch on bridge arm 3 has no action.

Because the switch Q_1 is turned off, the input voltage V_{AB} of tank circuit 1 starts to drop from V_{in} and the resonant current I_{r1} also starts to drop rapidly. Although the resonant current I_{r2} in tank circuit 2 also decreases at this time, the V_{CB} does not change, so the resonant current I_{r2} decreases at a lower speed than I_{r1} . The difference in the descending slopes of the two resonant currents makes the rectified current transmitted by tank circuit 1 to the secondary side of the transformer smaller than that of tank circuit 2. To satisfy Kirchhoff's current law, the rectifier diode D_{R3} on the secondary side is turned on to play a shunt. When D_{R3} is turned on, the secondary side of tank circuit 1 is short-circuited, the clamping voltage across the excitation inductance L_{m1} drops from $nV_{out}/2$ to 0, and the excitation current I_{m1} no longer increases. The clamping voltage across the excitation inductor L_{m2} rises from $nV_{out}/2$ to nV_{out} , and the excitation current I_{m2} rises faster. The input of tank circuit 2 does not change, but the clamping voltage of L_{m2} increases, which explains why I_{r2} also decreases.

5. In the $[t_1, t_2]$ stage (Figure 9e) at the time of t_1 , switch Q_2 is turned on at zero voltage, $V_{AB} = 0$ and resonance tanks 1 and 2 continue to resonate. However, because the output of tank circuit 1 is short-circuited, only tank circuit 2 transmits energy to the secondary side during this period. The expressions of v_{cr1} , v_{cr2} , i_{r1} , i_{r2} , i_{m1} , i_{m2} in this stage are as follows.

Tank circuit 1:

$$v_{cr1}(t) = i_{r1}(t_1) \cdot \sqrt{\frac{L_{r1}}{C_{r1}}} \cdot \sin\left[\sqrt{\frac{1}{L_{r1} \cdot C_{r1}}}(t - t_1)\right] + v_{cr1}(t_1) \cdot \cos\left[\sqrt{\frac{1}{L_{r1} \cdot C_{r1}}}(t - t_1)\right] \quad (4)$$

$$i_{r1}(t) = i_{r1}(t_1) \cdot \cos\left[\sqrt{\frac{1}{L_{r1} \cdot C_{r1}}}(t - t_1)\right] - v_{cr1}(t_1) \cdot \sqrt{\frac{C_{r1}}{L_{r1}}} \cdot \sin\left[\sqrt{\frac{1}{L_{r1} \cdot C_{r1}}}(t - t_1)\right] \quad (5)$$

$$i_{m1}(t) = i_{m1}(t_1) \quad (6)$$

Tank circuit 2:

$$v_{cr2}(t) = V_{in} - n \cdot V_{out} + i_{r2}(t_1) \cdot \sqrt{\frac{L_{r2}}{C_{r2}}} \cdot \sin\left[\sqrt{\frac{1}{L_{r2} \cdot C_{r2}}}(t - t_1)\right] + [v_{cr2}(t_1) - (V_{in} - n \cdot V_{out})] \cdot \cos\left[\sqrt{\frac{1}{L_{r2} \cdot C_{r2}}}(t - t_1)\right] \quad (7)$$

$$i_{r2}(t) = i_{r2}(t_1) \cdot \cos\left[\sqrt{\frac{1}{L_{r2} \cdot C_{r2}}}(t - t_1)\right] - [v_{cr2}(t_1) - (V_{in} - n \cdot V_{out})] \cdot \sqrt{\frac{C_{r2}}{L_{r2}}} \cdot \sin\left[\sqrt{\frac{1}{L_{r2} \cdot C_{r2}}}(t - t_1)\right] \quad (8)$$

$$i_{m2}(t) = i_{m2}(t_1) + \frac{n \cdot V_{out}}{L_{m2}} \cdot (t - t_1) \quad (9)$$

6. $[t_2, t_3]$ stage (Figure 9f) at time t_2 , the resonant current I_{r1} in tank circuit 1 is equal to the excitation current I_{m1} , the excitation inductance L_{m1} participates in the resonance, and rectifier diode D_1 is turned off at zero current. Tank circuit 2 is still in the resonant state, and all the currents transmitted by the secondary side of the transformer are

transmitted to the load side through the diodes D_2 and D_6 . The expressions of v_{cr1} , v_{cr2} , i_{r1} , i_{r2} , i_{m1} , i_{m2} in this stage are as follows.

Tank circuit 1:

$$v_{cr1}(t) = i_{r1}(t_2) \cdot \sqrt{\frac{L_{r1} + L_{m1}}{C_{r1}}} \cdot \sin\left[\sqrt{\frac{1}{(L_{r1} + L_{m1}) \cdot C_{r1}}}(t - t_2)\right] + v_{cr1}(t_2) \cdot \cos\left[\sqrt{\frac{1}{(L_{r1} + L_{m1}) \cdot C_{r1}}}(t - t_2)\right] \quad (10)$$

$$i_{r1}(t) = i_{m1}(t) = i_{r1}(t_2) \cdot \cos\left[\sqrt{\frac{1}{(L_{r1} + L_{m1}) \cdot C_{r1}}}(t - t_2)\right] - v_{cr1}(t_2) \cdot \sqrt{\frac{C_{r1}}{L_{r1} + L_{m1}}} \cdot \sin\left[\sqrt{\frac{1}{(L_{r1} + L_{m1}) \cdot C_{r1}}}(t - t_2)\right] \quad (11)$$

The expression of each state variable in resonance tank 2 is consistent with the previous stage.

- In the $[t_3, t_4]$ stage (Figure 9g), resonant current I_{r2} in tank circuit 2 at the time of t_3 is equal to the excitation current I_{m2} , and the excitation inductance L_{m2} participates in the resonance. So far, the two transformers are cut off from the secondary side. The primary and secondary sides of the circuit no longer have energy transfer and the load is powered by the output capacitor.

The expression of each state variable in resonance tank 1 is consistent with the previous stage.

Tank circuit 2:

$$v_{cr2}(t) = V_{in} + i_{r1}(t_3) \cdot \sqrt{\frac{L_{r2} + L_{m2}}{C_{r2}}} \cdot \sin\left[\sqrt{\frac{1}{(L_{r2} + L_{m2}) \cdot C_{r2}}}(t - t_3)\right] + [v_{cr2}(t_3) - V_{in}] \cdot \cos\left[\sqrt{\frac{1}{(L_{r2} + L_{m2}) \cdot C_{r2}}}(t - t_3)\right] \quad (12)$$

$$i_{r2}(t) = i_{m2}(t) = i_{r2}(t_3) \cdot \cos\left[\sqrt{\frac{1}{(L_{r2} + L_{m2}) \cdot C_{r2}}}(t - t_3)\right] - [v_{cr2}(t_3) - V_{in}] \cdot \sqrt{\frac{C_{r2}}{L_{r2} + L_{m2}}} \cdot \sin\left[\sqrt{\frac{1}{(L_{r2} + L_{m2}) \cdot C_{r2}}}(t - t_3)\right] \quad (13)$$

Through the above analysis, it can be obtained that in the half-bridge phase-shift mode, the active switch in the topology has zero-voltage turn-on capability, and the rectifier diode can achieve zero-current turn-off.

3. Gain Analysis

Among the gain analysis methods of resonant converters, the most commonly used is the fundamental wave analysis method (first harmonic approximation, FHA) [9,10]. In FHA, the input square wave voltage of the tank circuit is approximately regarded as its fundamental wave component and its higher harmonics are ignored, and the load R_L is converted to the primary side $R_{ac} = 4n^2R_L/\pi^2$ under the assumption that the secondary side rectified current is a sine wave, so that the tank circuit in the main circuit is transformed into an equivalent model as shown in Figure 10.

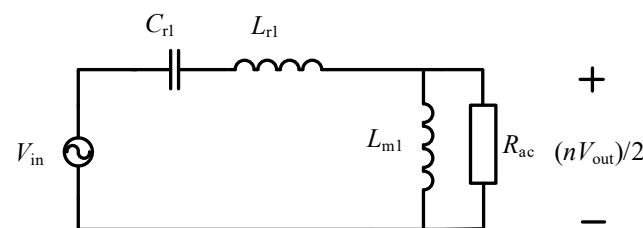


Figure 10. Equivalent circuit diagram of LLC resonant tank.

According to the equivalent circuit diagram, the analytical expressions of the gain of the converter in the full-bridge FM mode and the half-bridge FM mode can be listed.

Full-bridge FM:

$$M_{FB_VF} = \frac{nV_{out}}{V_{in}} \frac{2}{\sqrt{\left(1 + \frac{1}{h} - \frac{1}{f_n^2 h}\right)^2 + Q^2 \left(f_n - \frac{1}{f_n}\right)^2}} \quad (14)$$

Half-bridge FM:

$$M_{HB_VF} = \frac{nV_{out}}{V_{in}} \frac{1}{\sqrt{\left(1 + \frac{1}{h} - \frac{1}{f_n^2 h}\right)^2 + Q^2 \left(f_n - \frac{1}{f_n}\right)^2}} \quad (15)$$

where $Q = Z_r/R_{ac}$ represents the quality factor, $h = L_m/L_r$ represents the inductance ratio, $f_n = f_s/f_r$ represents the normalized frequency, f_s is the switching frequency and f_r is the resonant frequency.

Through the analytical expression of gain, we can draw the DC gain curves in full-bridge FM mode and half-bridge FM mode, as shown in Figures 11 and 12, respectively.

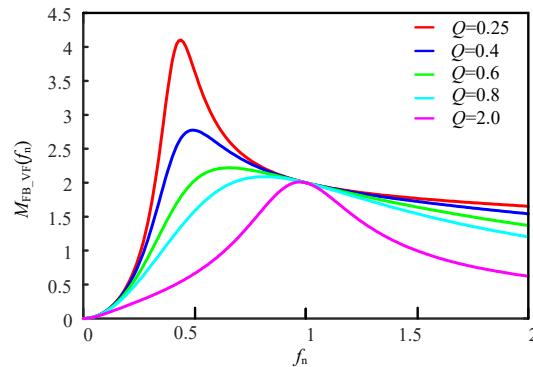


Figure 11. M_{FB_VF} gain curve in full-bridge FM mode.

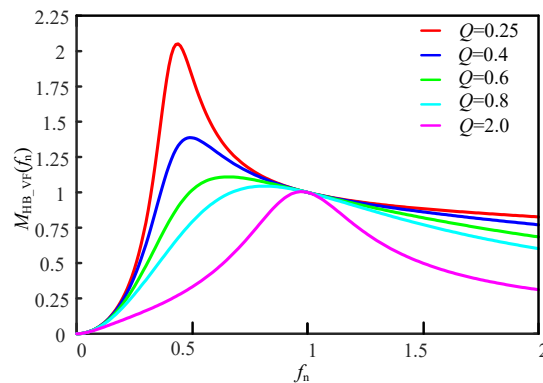


Figure 12. M_{HB_VF} gain curve in half-bridge FM mode.

When the resonant converter adopts the fixed-frequency and phase-shift control, the harmonic content increases, and the continuous use of the fundamental wave analysis method will cause a large error. Therefore, in the gain analysis of the full-bridge phase-shift mode and the half-bridge phase-shift mode, the time domain analysis method is used to write the time domain expressions of each state quantity in the tank circuit in different stages, and the calculation software can be used to draw the DC gain curves of the full-bridge phase-shift mode and the half-bridge phase-shift mode are shown in Figures 13 and 14.

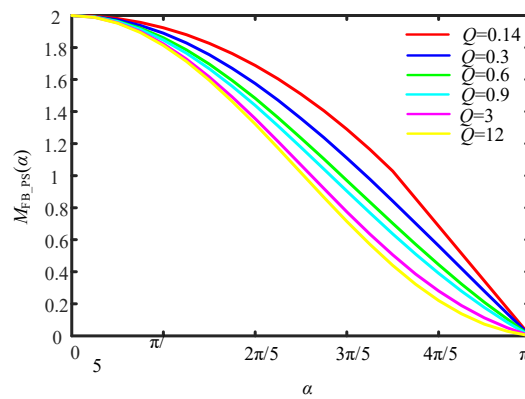


Figure 13. M_{FB_PS} gain curve in full-bridge phase-shift mode.

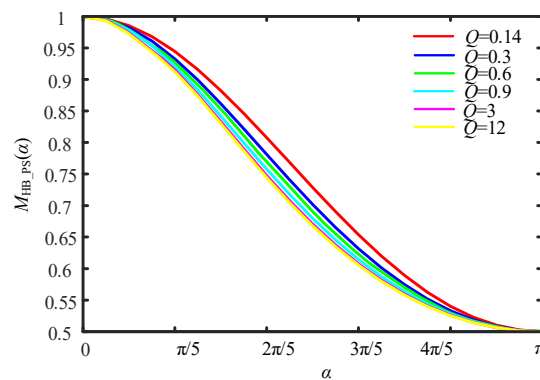


Figure 14. M_{HB_PS} gain curve in half-bridge phase-shift mode.

When the circuit works in full-bridge FM or half-bridge FM mode, the switching frequency f_s always works below the resonant frequency f_r . When $f_s > f_r$, the rectifier diode on the secondary side of the transformer loses the ability to turn off zero current. In the full-bridge phase-shift and half-bridge phase-shift modes, the switching frequency $f_s = f_r$ is set to maintain the high efficiency of the efficient transmission. Combined with the above gain analysis, the overall gain curve of the multi-mode switching wide-output resonant converter proposed in this paper is obtained, as shown in Figure 15.

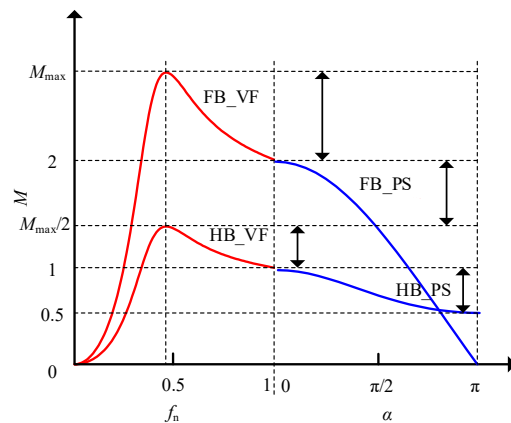


Figure 15. The overall gain curve of the new wide-output resonant converter.

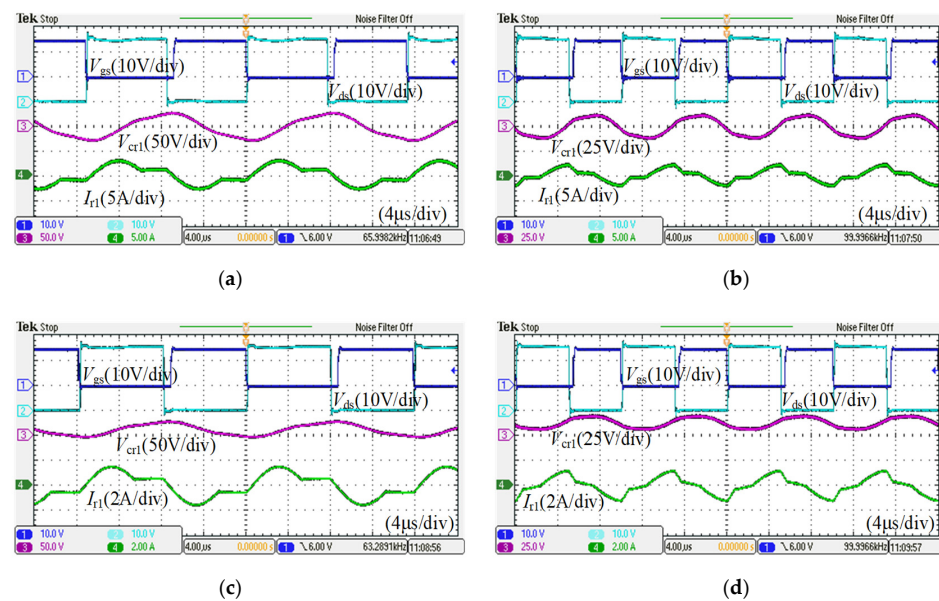
4. Experiment Verifications

To verify the wide output capability and soft switching characteristics of the novel resonant converter proposed in this paper, a 100 W experimental prototype was built. Table 1 lists the main parameters of the experimental prototype.

Table 1. Key Parameters of Resonant Converters.

Basic Parameters	Value
Input voltage V_{in} (Vdc)	25
Output voltage V_{out} (Vdc)	9–35
Resonance frequency f_r (kHz)	100
Specified load R_L (Ω)	12.5
Resonant capacitor C_r (μ F)	0.204
Resonant inductor L_r (μ H)	12.42
Excitation inductance L_m (μ H)	74.5
Ratio of transformer n	2:1

The experimental waveform shown in Figure 16 includes the resonant current I_{r1} in tank circuit 1, the resonant capacitor voltage V_{cr1} , the driving voltage V_{gs} across the switching transistor Q_2 GS and the voltage V_{ds} across the DS. As can be seen from the figure, before V_{gs} rises from 0 to 15 V, V_{ds} has dropped to 0, and the current value corresponding to the resonant current I_{r1} at this moment is positive, which flows through the anti-parallel diode of the power switch. Experiments show that, under the four operating modes, the power switch on the primary side can achieve zero-voltage turn-on capability.

**Figure 16.** ZVS experimental verification waveform. (a) Full-bridge FM mode; (b) full-bridge phase-shift mode; (c) half-bridge FM mode; (d) half-bridge phase-shift mode.

The experimental waveforms shown in Figure 17 include the resonant capacitor voltage V_{cr1} in tank circuit 1 and the secondary current I_{s1} of transformer T_1 . In the frequency modulation mode, the operating frequency of the switch is greater than the resonant frequency and, within a switching cycle, the resonant current will periodically drop to the size of the excitation current, and there is no current difference between the two, so the secondary current I_{s1} refracted to the transformer is also 0, as shown in Figure 17a,c. In the phase-shift mode, although the switching frequency is fixed at the resonant frequency, because of the existence of the phase-shift angle, the resonant current will decrease in advance and the rectified current can also naturally decrease to 0, as shown in Figure 17b,d. Experiments show that under the four operating modes, the rectifier diodes on the secondary side can achieve zero-current turn-off capability.

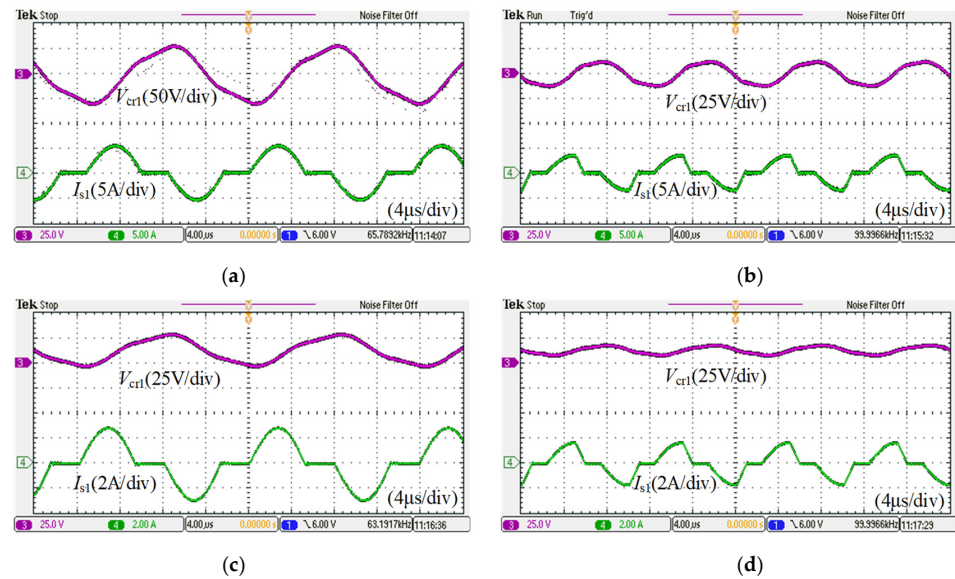


Figure 17. ZCS experimental verification waveform. (a) Full-bridge FM mode; (b) full-bridge phase-shift mode; (c) half-bridge FM mode; (d) half-bridge phase-shift mode.

Figure 18 shows the upper and lower limits of the required output voltage in each mode when the input voltage is fixed. The experimental waveforms shown in the figure include the output voltage V_{out} and the resonant capacitor voltage V_{cr1} in tank 1. In the full-bridge frequency modulation mode, the controller changes the output voltage by adjusting the frequency and the circuit belongs to the boost state. The maximum output of the circuit can reach 35 V, as shown in Figure 18a. At this time, the resonant capacitor voltage V_{cr1} is in a sinusoidal state, the maximum amplitude is 50 V, and the switching frequency $f_s = 52$ kHz; when the switching frequency rises to the resonant frequency f_r , the output voltage $V_{out} = 24$ V and the capacitor voltage V_{cr1} amplitude is 15 V, as shown in Figure 18b. This is due to the turn-on voltage drop that exists in the circuit, which makes the circuit's voltage gain at the resonant frequency less than ideal.

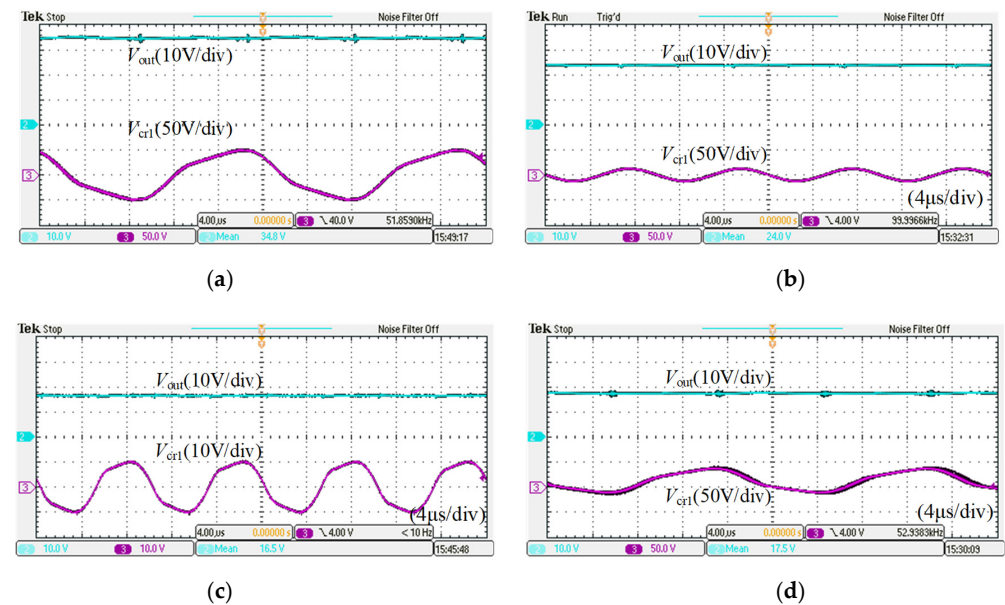


Figure 18. Cont.

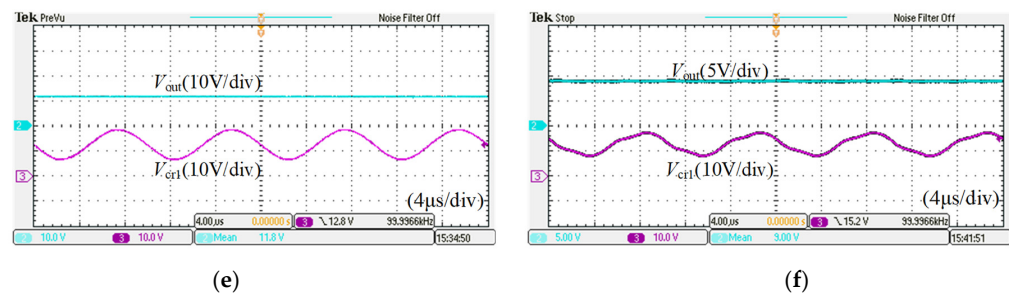


Figure 18. Wide-output experimental verification waveform. (a) $V_{out} = 35$ V; (b) $V_{out} = 24$ V; (c) $V_{out} = 16.5$ V; (d) $V_{out} = 17.5$ V; (e) $V_{out} = 11.8$ V; (f) $V_{out} = 9$ V.

The lower limit of the output voltage in the full-bridge frequency modulation mode is also the output upper limit of the full-bridge phase-shift mode, and the phase-shift angle is 0. The controller can continue to reduce the voltage by increasing the phase-shift angle. When the output voltage $V_{out} = 16.5$ V, the lower limit of the output voltage of the full-bridge phase-shift mode is reached, as shown in Figure 18c. The phase-shift angle $\alpha = 0.54\pi$ and the amplitude of the resonant capacitor voltage V_{cr1} is 10 V.

The upper limit of the output voltage in the half-bridge FM mode is set to 17.5 V, as shown in Figure 18d. The circuit switching frequency $f_s = 53$ kHz, the resonant capacitor voltage V_{cr1} is a sine wave with a DC offset of 12.5 V and its amplitude is 25 V; when the switching frequency reaches the resonant frequency, the output voltage $V_{out} = 11.8$ V and the amplitude of the resonant capacitor voltage V_{cr1} is 6 V, as shown in Figure 18e.

In the design requirements, the lower limit voltage that the half-bridge phase-shift mode needs to reach is 9 V. At this time, the phase-shift angle $\alpha = 0.52\pi$ and the amplitude of the resonant capacitor voltage V_{cr1} is 5 V, as shown in Figure 18f. The experimental results show that the experimental prototype meets the wide output range required by the design.

5. Conclusions

In this paper, a new type of wide-output resonant converter is proposed. The rectifier side of the transformer secondary side adopts a new type of series-parallel self-adjusting rectifier structure. Compared with the traditional LLC resonant converter topology, a new operating mode is added. Therefore, the gain range of the entire circuit is expanded. In addition, the switching frequency of the resonant circuit always maintains $f_s \leq f_r$. In the four operating modes, the active switches on the primary side of the transformer can be turned on at zero voltage, and the rectifier diodes on the secondary side can be turned off at zero current, maintaining the low-loss characteristics of traditional LLC resonant converters. The analysis of the working principle and the experimental results fully prove this conclusion.

Author Contributions: Conceptualization, X.Z.; Data curation, Y.G.; Formal analysis, Y.G.; Funding acquisition, Y.G.; Investigation, Y.G. and X.Z.; Methodology, X.Z.; Resources, Y.G., X.Z., Z.J. and A.L.; Validation, Z.J.; Writing—review & editing, B.W. All authors have read and agreed to the published version of the manuscript.

Funding: This research received no external funding.

Data Availability Statement: The study did not report any data.

Conflicts of Interest: The authors declare no conflict of interest.

References

1. Maniktala, S. *Switching Power Supplies A to Z*; Elsevier: Amsterdam, The Netherlands, 2006; pp. 37–39.
2. Erickson, R.; Maksimovic, D. *Fundamentals of Power Electronics*, 2nd ed.; Kluwer Academic Publishers: New York, NY, USA, 2001; pp. 45–46.

3. Lee, I.O.; Cho, S.Y.; Moon, G.W. Interleaved Buck Converter Having Low Switching Losses and Improved Step-Down Conversion Ratio. *IEEE Trans. Power Electron.* **2012**, *27*, 3664–3675. [[CrossRef](#)]
4. Karppanen, M.; Arminen, J.; Suntio, T.; Savela, K.; Simola, J. Dynamical Modeling and Characterization of Peak-Current-Controlled Superbuck Converter. *IEEE Trans. Power Electron.* **2008**, *23*, 1370–1380. [[CrossRef](#)]
5. Leppäaho, J.; Suntio, T. Dynamic Characteristics of Current-Fed Superbuck Converter. *IEEE Trans. Power Electron.* **2011**, *26*, 200–209. [[CrossRef](#)]
6. Roinila, T.; Hankaniemi, M.; Suntio, T.; Sippola, M.; Vilkkö, M. Dynamical profile of a switched-mode converter-reality or imagination. In Proceedings of the IEEE International Telecommunications Energy Conference, Rome, Italy, 30 September–4 October 2007; pp. 420–427.
7. Suntio, T. Unified small-signal modeling of direct-on-time control. *IEEE Trans. Indus. Electron.* **2006**, *53*, 287–295. [[CrossRef](#)]
8. Freudenberg, J.S.; Looze, D.P. Right half plane poles and zeros and design tradeoffs in feedback systems. *IEEE Trans. Autom. Control* **1985**, *30*, 555–565. [[CrossRef](#)]
9. Suntio, T.; Hankaniemi, M.; Karppanen, M. Analysing the dynamics of regulated converters. *IEE Proc. Electr. Power Appl.* **2006**, *153*, 905–910. [[CrossRef](#)]
10. Cuk, S.; Polivka, W.M. Analysis of integrated magnetics to eliminated current ripple in switching converters. In Proceedings of the 6th Power Conversion International Conference, Orlando, FL, USA, 19–21 April 1983; pp. 361–386.